doi:10.1016/S0022-2836(02)00858-6 available online at http://www.idealibrary.com on IDEAL® J. Mol. Biol. (2002) 322, 943–954

JMB

Myxoma Virus Immunomodulatory Protein M156R is a Structural Mimic of Eukaryotic Translation Initiation Factor eIF2α

Theresa A. Ramelot[1], John R. Cort[1], Adelinda A. Yee[2,3], Furong Liu[4] Michael B. Goshe[1], Aled M. Edwards[2,3], Richard D. Smith[1] Cheryl H. Arrowsmith[2,3], Thomas E. Dever[4] and Michael A. Kennedy[1]*

[1]*Environmental Molecular Sciences Laboratory, Pacific Northwest National Laboratory K8-98, Richland, WA 99352 USA*

[2]*Division of Molecular and Structural Biology Ontario Cancer Institute Toronto, Ontario, Canada*

[3]*Department of Medical Biophysics, University of Toronto, 101 College Street Toronto, Ontario, Canada M5G 1L7*

[4]*Laboratory of Gene Regulation and Development, National Institutes of Health, Bethesda MD 20892-2716, USA*

**Corresponding author*

Phosphorylation of the translation initiation factor eIF2 on Ser51 of its α subunit is a key event for regulation of protein synthesis in all eukaryotes. M156R, the product of the myxoma virus M156R open reading frame, has sequence similarity to eIF2α as well as to a family of viral proteins that bind to the interferon-induced protein kinase PKR and inhibit phosphorylation of eIF2α. In this study, we demonstrate that, like eIF2α. M156R is an efficient substrate for phosphorylation by PKR and can compete with eIF2α. To gain insights into the substrate specificity of the eIF2α kinases, we have determined the nuclear magnetic resonance (NMR) structure of M156R, the first structure of a myxoma virus protein. The fold consists of a five-stranded antiparallel β-barrel with two of the strands connected by a loop and an α-helix. The similarity between M156R and the β-barrel structure in the N terminus of eIF2α suggests that the viral homologs mimic eIF2α structure in order to compete for binding to PKR. A homology-modeled structure of the well-studied vaccinia virus K3L was generated on the basis of alignment with M156R. Comparison of the structures of the K3L model, M156R, and human eIF2α indicated that residues important for binding to PKR are located at conserved positions on the surface of the β-barrel and in the mobile loop, identifying the putative PKR recognition motif.

Keywords: eIF2α; K3L; myxoma virus M156R; nuclear magnetic resonance; PKR

Introduction

The open reading frame M156R, located immediately adjacent to the right-hand terminally inverted repeat (TIR) of the myxoma virus genome, encodes a 12 kDa putative immunomodulatory protein. Myxoma virus, which is a member of the *Leporipoxvirus* genus, Chrodopoxvirinae subfamily, in the Poxviridae family, is a dsDNA virus that causes lethal myxomatosis in European rabbits. Myxoma virus, like other members of the poxvirus family, contains several genes that encode well-characterized, host-related immunomodulatory proteins. In the recently sequenced myxoma virus genome (strain Lausanne), M156R is one of several new putative immunomodulatory proteins that were identified by their similarity to host proteins or homologs found in other viruses.[1,2] These viral proteins mimic host cell proteins in order to compromise antiviral defense mechanisms.[3,4]

Sequence comparison to M156R with the program BLASTp revealed sequence homology to two viral proteins with known immunomodulatory functions.[1] The swinepox virus C8L protein is 39% identical with M156R (26/66 residues) and the vaccinia virus K3L protein is 33% identical (20/60). Both homologs act as inhibitors of the interferon-inducible dsRNA-dependent protein kinase, PKR.[5–9] This was first

A.M.E., C.H.A. and M.A.K. are members of the Northeast Structural Genomics Consortium.

Abbreviations used: TIR, terminally inverted repeat; ds-, double-stranded; ss-, singe-stranded; eIF, eukaryotic translation initiation factor; OB, oligonucleotide/oligosaccharide-binding; NOE, nuclear Overhauser enhancement; LC-MS/MS, liquid chromatography-tandem mass spectrometry.

E-mail address of the corresponding author: ma_kennedy@pnl.gov

0022-2836/02/$ - see front matter

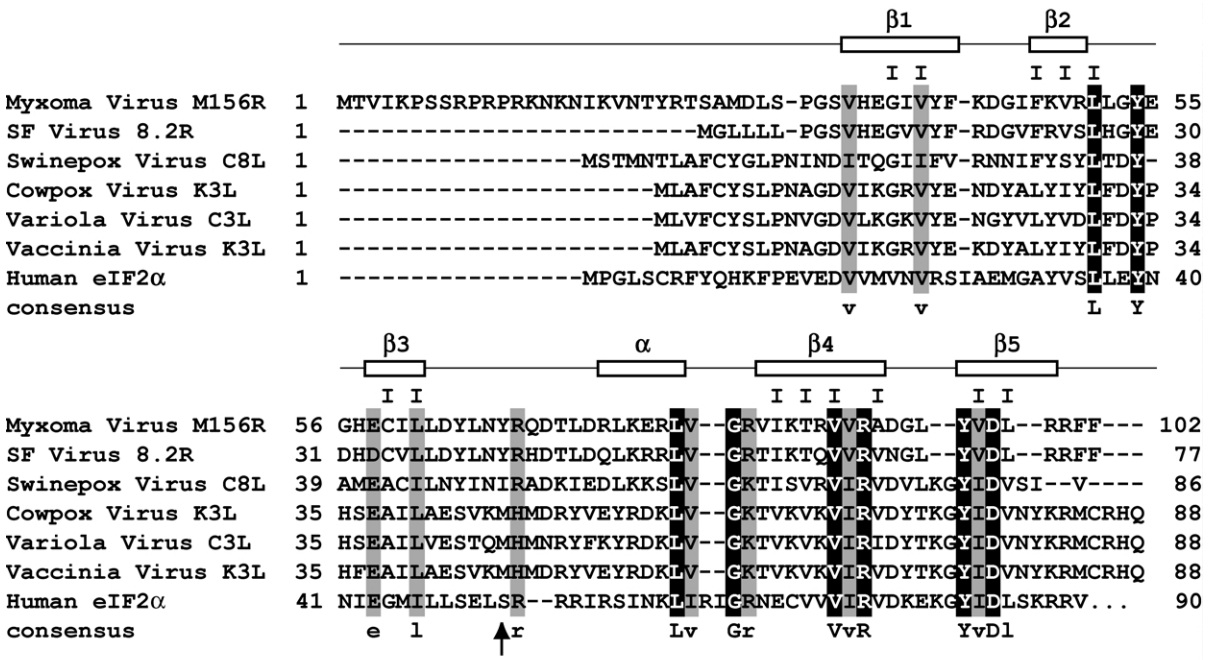

Figure 1. Multiple sequence alignment of myxoma virus M156R, other viral homologs, and human eIF2α. Sequences are from myxoma virus M156R (strain Lausanne; Genbank accession number AF170726[1]), shope (rabbit) fibroma virus gp008.2L (AF170722[55]), swinepox virus C8L (strain Kasza; L22013[56]), vaccinia virus K3L (strain WR; WMVZK2[57]), cowpox virus K3L (X83621), variola virus C3L (strain India-1967; X69198[58]), and residues 1–90 of human eIF2α (J02645[59]). Residues in M156R that have side-chains inside the barrel are indicated by an I above. The S51 phosphorylation site in eIF2α is indicated by an arrow. The eIF2α phosphorylation site is referred to here and in the literature as S51 rather than S52, due to post-translational removal of the first Met in mammalian eIF2α.

discovered for K3L, which resembles the N-terminal one-third of the eukaryotic translation initiation factor 2α (eIF2α).[5,8] In the antiviral response, PKR is transcriptionally induced by interferon and becomes activated by dsRNA produced during viral infection. The active PKR subsequently phosphorylates eIF2α, resulting in translational inhibition that prevents synthesis of viral proteins. By competing with eIF2α for binding to PKR, these viral inhibitors allow protein synthesis to continue. Binding to PKR has been demonstrated for both K3L and C8L, and both viral proteins can reverse the translational inhibition that results from phosphorylation of eIF2α in mammalian cells.[6,8–11]

Phosphorylation of Ser51 on the α subunit of the heterotrimeric translation initiation factor eIF2 is a primary regulator of mRNA translation. The first step of translation initiation is the binding of the ternary complex of eIF2, GTP, and initiator Met-tRNA to the 40 S ribosomal subunit. This 43 S preinitiation complex with the assistance of additional factors binds to mRNA. Following ribosomal scanning and recognition of the initiator AUG codon, the GTP bound to eIF2 is hydrolyzed to GDP. The eIF2 is then released from the ribosome in an inactive GDP-bound form. GDP is replaced with GTP by eIF2B, a guanine nucleotide exchange factor, allowing subsequent rounds of translation initiation. In response to viral invasion, the kinase PKR is activated and phosphorylates eIF2α, inhibiting the nucleotide exchange reaction. The resulting phosphorylation of Ser51 of eIF2α increases the affinity of GDP bound eIF2 for eIF2B, resulting in an inactive complex.[12] Since eIF2B concentrations are limiting, phosphorylation of only a fraction of eIF2α will inhibit the guanine nucleotide exchange reaction and block total translation initiation.[12] In order to prevent shutdown of protein synthesis, many viruses express inhibitors of PKR,[13] including eIF2α homologs found in poxviruses that can bind to PKR, resulting in decreased phosphorylation of eIF2α.

In addition to PKR, three other eukaryotic protein kinases are known that can modulate protein synthesis by phosphorylation of eIF2α. All four kinases contain a conserved eIF2α kinase domain along with different regulatory domains, so that each kinase regulates translation initiation in response to different cellular stresses (reviewed by Dever[14]). For example, the heme-regulated inhibitor kinase (HRI) phosphorylates eIF2α in response to heme depletion and the general control non-derepressible-2 kinase (GCN2) is activated in response to amino acid starvation. The fourth kinase, pancreatic eIF2α kinase (PEK or PERK) is activated in response to endoplasmic reticulum stress as part of the unfolded protein response.[15] Vaccinia virus K3L is a demonstrated inhibitor of each of the known eIF2α kinases,[6,8,16–18] suggesting that by mimicking eIF2α, viral inhibitors can modulate translational control over a wide range

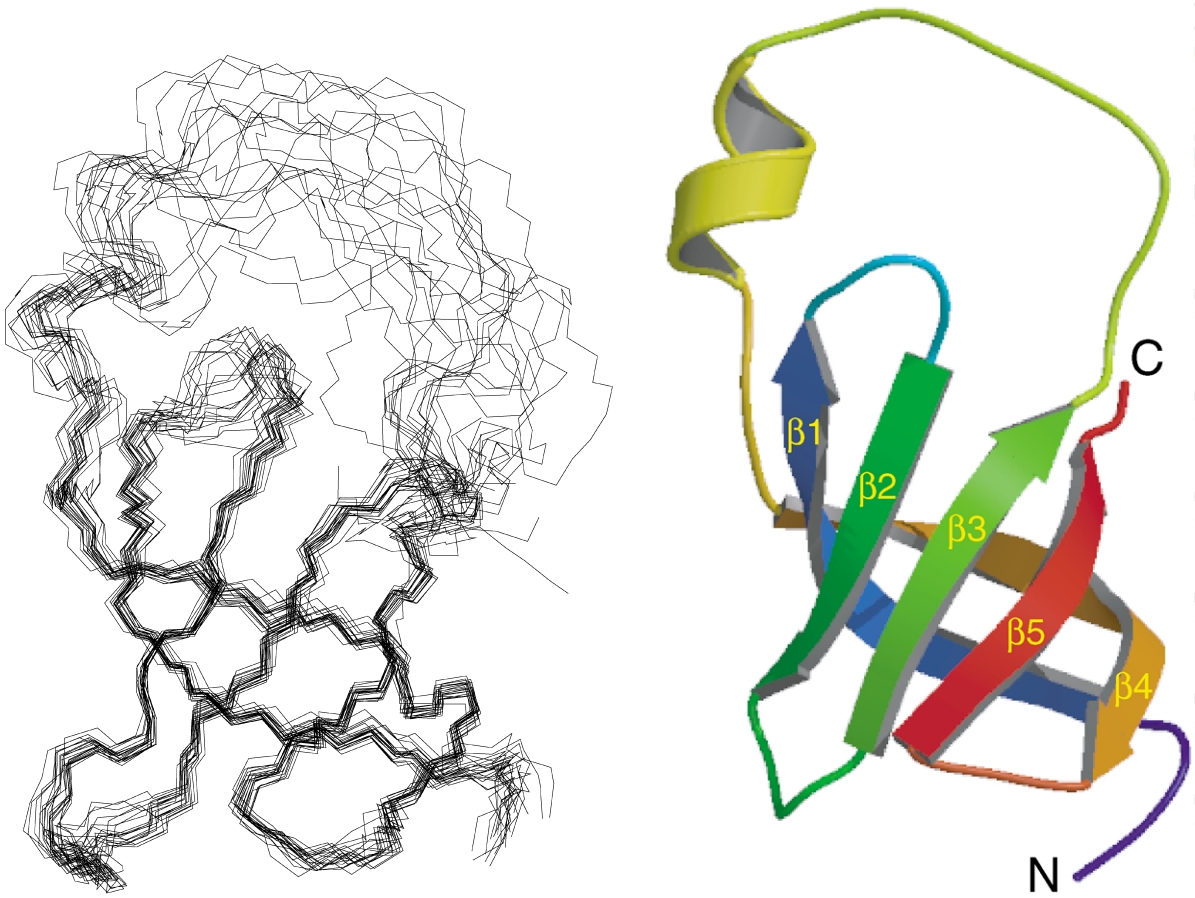

Figure 2. (a) Backbone (N, C^{α}, and C′) atoms of 20 NMR structures (residues 32–102) optimally superimposed with respect to the average coordinates of the backbone atoms of residues 33–61 and 74–100. (b) Ribbon representation of M156R structure (residues 30–102) with the β-strands labeled as in Figure 1.

of conditions. Specifically, repression of PKR is an important viral mechanism for avoiding the antiviral effects of the host interferon response.

There is no structure for a viral pseudosubstrate inhibitor of PKR in the Protein Data Bank. However, a recent structure of the N-terminal segment of human eIF2α, has been determined.[19] The first domain of eIF2α contains an oligonucleotide/oligosaccharide-binding (OB) fold. Vaccinia virus K3L is also predicted to have this fold, sometimes called an S1 domain.[20] K3L and C8L are both sequence homologs of eIF2α with 27–28% identity with the first 90 residues of human eIF2α, whereas M156R is even more divergent with only 19% identity (Figure 1). The greatest sequence similarity between these viral homologs and eIF2α is found for 19 residues near the C terminus of M156R with seven identically conserved residues. The sequences of the viral homologs are also markedly divergent, with only 14 residues that are identically conserved among all three proteins (Figure 1). To better understand how these sequence similarities are related to function of the viral homologs as PKR inhibitors, we determined the structure of M156R and tested the ability of M156R to function as a PKR substrate and/or inhibitor. Our results show that M156R is an efficient substrate for phosphorylation by PKR *in vitro* and that M156R can compete with eIF2α for phosphorylation by PKR. We found that M156R has the OB fold found in eIF2α. This suggests that M156R functions as a substrate for PKR by mimicking the cellular substrate, eIF2α. In addition, structural analysis identifies features that are conserved among the viral homologs and allows visualization of the PKR recognition motif on the basis of sequence alignment with eIF2α and other viral homologs.

Results

Solution structure of M156R

Structures of M156R were generated using distance and dihedral angle restraints (described in Materials and Methods). The backbone trace of the ensemble of 20 lowest-energy structures (residues 32–102) is shown in Figure 2(a) and a representative structure is shown in Figure 2(b). Residues 1–32, 62–73, and 101–102 were not restricted during superposition of the structures and were omitted from most of the statistical analysis (Table 1). The structures have an average r.m.s. deviation of 0.73 Å for backbone atoms, nuclear Overhauser

Table 1. Structural statistics for M156R final ensemble of 20 structures

Distance restraints	374
Intra-residue	0
Sequential	169
Medium ($1 < i < 5$)	44
Long-range ($i \geq 5$)	113
Hydrogen bond restraints (two per H-bond)	48
Dihedral restraints	66
ϕ	34
Ψ	32
Distance restraint violations	
Mean number of violations	35.7 ± 2.7
Mean r.m.s. violation (Å)	0.013 ± 0.002
Dihedral restraint violations	
Mean number of violations	10.1 ± 1.7
Mean r.m.s. violation (deg.)	0.46 ± 0.13
r.m.s. deviation from the average coordinates (Å)	
Residues 33–61, 83–100	
Backbone atoms (N, C^{α}, C′)	0.48 ± 0.08
All heavy-atoms	1.20 ± 0.14
Residues 33–61, 74–100	
Backbone atoms (N, C^{α}, C′)	0.73 ± 0.22
All heavy-atoms	1.52 ± 0.29
Ramachandran statistics (PROCHECK-NMR[60])	
Residues 33–61, 74–100	
Residues in most favored region (%)	79.3
Residues in additional allowed regions (%)	18.4
Residues in generously allowed regions (%)	1.8
Residues in disallowed regions (%)	0.5

enhancement (NOE) r.m.s. violation of 0.013, and only 0.5% of residues located in disallowed regions of the Ramachandran plot, indicating good quality (Table 1).

The structure contains 32 unstructured residues at the N terminus, one α-helix (residues 74–79) and five β-strands (residues 35–42, 47–50, 58–61, 83–91, and 95–99). The antiparallel β-strands are arranged in the order 3–2–1–4–5, with the first four strands in the Greek key topology. The structure forms a closed barrel because strands 3 and 5 form parallel β-strands. The β-barrel is a compact structure with a diameter of approximately 20–25 Å. Strands 1 and 4 are the longest and form large curves around the barrel. Strands 1 and 2, and strands 4 and 5, are connected by short loops of four and three residues, respectively, whereas the rest of the strands are connected by longer loops. Strands 2 and 3 are linked by a seven-residue loop and strands 3 and 4 are separated by 21 residues. The linker between strands 3 and 4 lies at the end of the barrel and contains a short six residue α-helix preceding strand 4. Residues 62–73 of the loop preceding the α-helix had few structural restraints and this sequence therefore has a large variability in structural coordinates among the ensemble of structures.

The secondary structure of M156R is shown along with the sequence alignment of M156R, other viral homologs, and eIF2α (Figure 1). The interior of the barrel contains mostly Leu and Val and other aliphatic side-chains and contains no aromatic side-chains. These residues have predominantly conservative substitutions of Leu, Val, Ile, Gly, and Ala in the aligned proteins sequences. Gly residues 33, 45, 53, 56, and 81, which are located in loops, adopt α_L (left-handed α-helix) backbone conformations. G81 is the third residue of a four-residue reverse turn and is the only Gly conserved in all the aligned sequences. There is little sequence similarity to any of the residues before strand 1 in M156R.

Phosphorylation of M156R by PKR

Sequence homology between C8L, K3L, and M156R suggested that M156R would also function as an inhibitor of PKR during viral invasion. However, in contrast to K3L, which can readily suppress the growth inhibition caused by PKR expression in yeast cells, M156R failed to inhibit PKR in the yeast assay (data not shown). Similarly, yeast two-hybrid assays readily detected an interaction between PKR and K3L, but no interaction was observed between PKR and M156R (data not shown). As the two-hybrid assay also failed to detect an interaction between PKR and its substrate eIF2α (data not shown), the negative result for M156R does not preclude M156R as a substrate. To test whether PKR can phosphorylate M156R, *in vitro* kinase assays were performed using purified recombinant PKR, eIF2α, and M156R. As shown in Figure 3(a) (lanes 1–3), PKR readily phosphorylated eIF2α. PKR is known to phosphorylate eIF2α exclusively on S51, and the *in vitro* assay displayed this same specificity, as an eIF2α-S51A protein was not an efficient substrate for PKR phosphorylation (Figure 3(a), lanes 8–10). The low level of phosphorylation seen in for eIF2α-S51A is likely due to a low level of non-specific phosphorylation by PKR. Interestingly, PKR was able to phosphorylate M156R as efficiently as it phosphorylated eIF2α (Figure 3(a), compare lanes 4–6 with lanes 1–3). Thus, consistent with its amino acid sequence similarity with eIF2α, M156R is a good substrate for PKR phosphorylation.

As most, if not all, viruses have developed means to inhibit PKR, it was of interest to determine whether M156R could block eIF2α phosphorylation through substrate competition. The *in vitro* kinase assays were repeated using the same small amount of PKR and roughly a 100-fold excess of eIF2α. Under these conditions of saturating substrate, addition of M156R resulted in a reduction of eIF2α phosphorylation (Figure 3(b), lanes 1–4). As the relative levels of eIF2α, M156R and PKR in infected cells is unknown, it is unclear whether this type of substrate competition is ever achieved during viral infection. However, these results suggest that M156R and eIF2α interact in a similar manner with PKR, consistent with the idea that M156R is an eIF2α homolog in myxoma virus.

Comparison of the amino acid sequences of eIF2α and M156R (Figure 1) reveals that Y67 in M156R is located at the position corresponding to S51 in eIF2α. We tested whether Y67 in M156R was important for PKR phosphorylation by mutating this residue to Ala. As shown in Figure

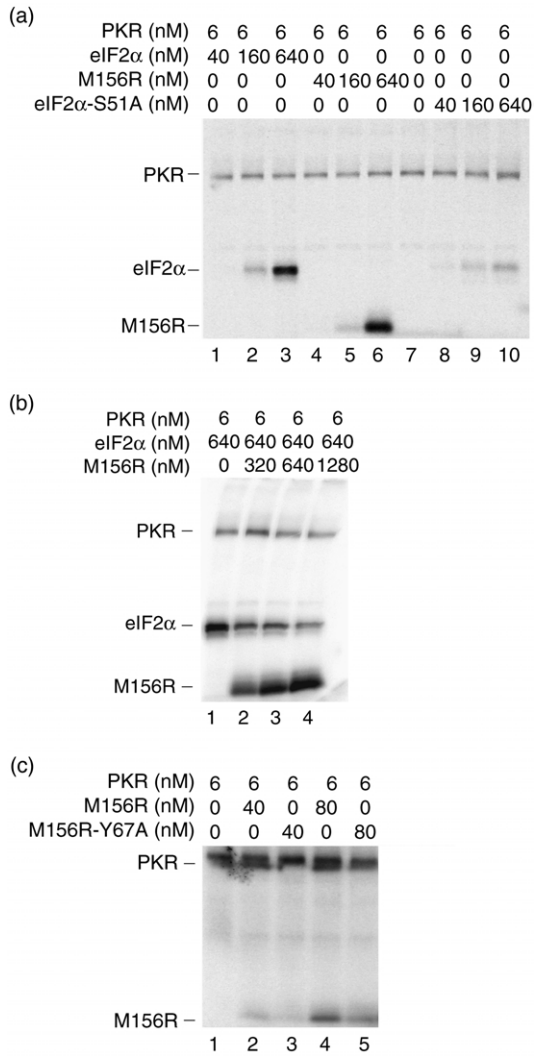

Figure 3. M156R is an efficient substrate of PKR. (a) *In vitro* kinase assays using [γ-^{33}P]ATP were performed using the indicated amounts of purified PKR, M156R, eIF2α, and eIF2α-S51A. Reaction products were analyzed by SDS/polyacrylamide gel electrophoresis followed by autoradiography. (b) Substrate competition between eIF2α and M156R for phosphorylation by PKR. *In vitro* kinase assays containing 6 nM PKR, 640 nM eIF2α, and the indicated concentrations of M156R were performed and analyzed as described. (c) PKR phosphorylation of M156R is critically dependent on Y67. Kinase reactions containing 6 nM PKR and the indicated concentrations of purified M156R or M156R-Y67A proteins were conducted and analyzed as described in Materials and Methods. The upper band is PKR and the bottom band is M156R or M156R-Y67A.

3(c), the M156R-Y67A mutant had significantly impaired phosphorylation by PKR (compare lanes 3 and 5 with lanes 2 and 4, respectively). Consistent with the idea that PKR phosphorylated M156R on Y67, phosphorylated wild-type M156R cross-reacted with anti-phosphotyrosine antibodies, and the M156R-Y67A mutant had significantly less crossreaction (data not shown). Liquid chromatography-tandem mass spectrometry (LC-MS/MS) analysis of *in vitro* phosphorylated M156R revealed that approximately 75% of the phosphorylation occurred in the peptide LLGYEGHECILLDYLNYR, which includes Y67. Fragmentation analysis indicated that Y54, Y64 or Y67 could be phosphorylated (data not shown). In addition, multiple phosphorylation sites were detected in the N terminus (residues 1–34). The identification of multiple PKR phosphorylation sites in M156R in addition to Y67 is consistent with the results in Figure 3(c) demonstrating that the Y67A mutation did not eliminate phosphorylation completely. Additional experimentation will be required to determine whether these alternative sites are phosphorylated *in vivo*. LC-MS/MS analysis of *in vitro* phosphorylated M156R-Y67A revealed a three- to fourfold decrease in phosphorylation of the aforementioned peptide containing the Y67A mutation. Taken together, our results demonstrate that M156R is an efficient substrate for PKR phosphorylation and, on the basis of the sequence similarity between M156R and eIF2α and the critical role of Y67 for M156R phosphorylation, we propose that M156R is an eIF2α mimic.

Modeling the PKR recognition motif

Mutagenesis studies of K3L indicate residues that are important for binding to PKR. Certain mutations in K3L increased the inhibition of PKR, while others prevented inhibition of PKR.[8] Binding studies and activity assays suggest that the H47R mutation increases the affinity of K3L for PKR, and C5G, K22E, F36S, and E37G mutations also enhanced K3L activity. Conversely, the Y76A mutation decreases the affinity and ability to inhibit PKR, and K74A and D78A mutations, as well as truncation at residues following K82, yielded a protein that was no longer able to inhibit PKR activity. The residues that were demonstrated by mutational studies to be important for PKR binding are shown on a homology model of K3L (Figure 4(a)). The homology model was generated on the basis of alignment with M156R and distance restraints derived from the structure of M156R using a simulated annealing method with restrained molecular dynamics.[21] Ten structures were generated with an average backbone r.m.s. deviation of 0.80(±0.19) Å for residues 11–83. Residues K74, Y76, D78, and K82 are located in or near strand 5 of K3L, K22 is located just after strand 1, F36 and E37 precede strand 3, while H47 is located in the loop after strand 3 and the top of the barrel (Figure 4(a)). These residues are all on one side of the barrel, suggesting a recognition motif for binding to PKR. On the basis of the sequence alignment, we suggest that the corresponding residues, K43, H57, E58, R68, Y95, D97, and R99, in M156R are involved in binding to PKR (Figure 4(b)).

Alignment of eIF2α and the viral homologs indicates several conserved residues (Figure 1). In addition to the conserved aliphatic residues inside the β-barrel, residues Y54, L79, G81, R90, Y95, and

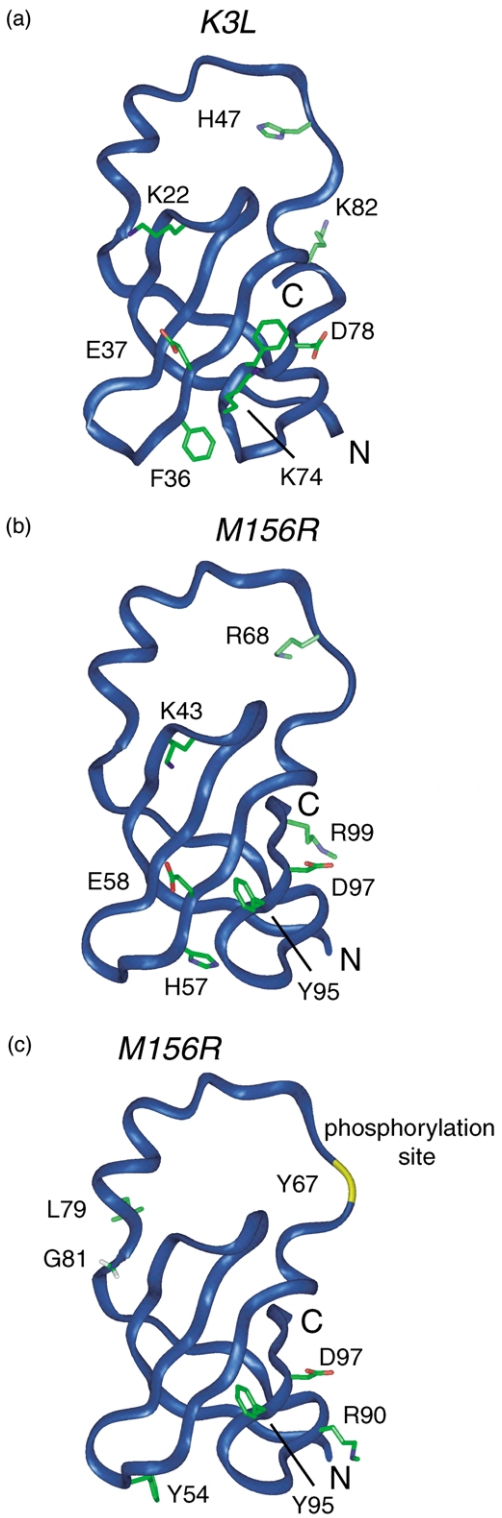

Figure 4. (a) Homology-modeled ribbon diagram of K3L (residues 11–83) showing the residues demonstrated by mutagenesis to affect PKR binding. C5 is not shown, since it is in the unstructured N terminus. (b) M156R ribbon diagram (residues 32–102) showing the residues implicated in binding to PKR, on the basis of alignment with K3L. (c) M156R ribbon diagram (residues 32–102) showing the identically conserved residues between eIF2α and the viral homologs of M156R and the phosphorylation site in yellow, which corresponds to the phosphorylation site S51 in eIF2α.

D97 in M156R are conserved. R90, Y95, and D97 are located in strands 4 and 5 near the previously described PKR-binding region. Y54 is in the loop between 2 and 3 near the bottom, while L79 and G81 are after the helix near the top of the barrel. These conserved residues are shown in Figure 4(c). In M156R, Y67, which is aligned with the PKR phosphorylation site in eIF2α, is located in the long linker between strands 3 and 4 at the top of the barrel, referred to as the phosphorylation loop. The location of residues conserved between eIF2α and the viral homologs suggests that a large surface of M156R is functionally important (Figure 4(c)).

The sequence KGYID, found near the C terminus of K3L and C8L, is part of the recognition sequence for binding to PKR.[8,9,11] This sequence is far from the corresponding eIF2α phosphorylation site, but may act as a docking site for the kinase.[8] *In vitro* binding studies show that deletion of this motif decreases binding with PKR and this deletion mutant can no longer compete with eIF2α for binding to PKR.[11] Likewise, substitution of Lys, Tyr, or Asp by Ala blocks K3L inhibition of PKR in yeast and the Tyr to Ala mutation reduces K3L binding to PKR.[8] In addition, an eIF2α mutant with GYID deleted exhibited reduced phosphorylation by PKR.[11] In M156R, only Tyr and Asp are conserved. Residues Y95 and D97, located in strand 5 of M156R along with other residues on the same face of the barrel and the aforementioned residues in the phosphorylation loop make up the putative recognition motif for PKR.

Although the viral homologs contain residues that are conserved with respect to eIF2α, there are differences that suggest that they do not depend on identical binding interactions with PKR for inhibition. For example, the K3L truncated after K82 was no longer able to inhibit PKR, whereas the shorter C8L, which is equivalent in length to the truncated K3L, acts as an effective inhibitor.[8,9] For the K3L truncation mutant, an additional mutation to H47R was able to re-establish activity.[8] This mutation makes K3L more like C8L and eIF2α, possibly explaining the increase in activity. However, the reciprocal mutation to R51H in C8L did not cause the expected decrease in activity, suggesting that additional interactions between C8L and PKR contribute significantly to binding.[9] K3L residue K74 was shown by mutational studies to be important for inhibition of PKR, but there is no corresponding residue in M156R because of a deletion in the loop between strands 4 and 5. Despite these differences, the electrostatic surface potentials of both M156R and K3L are very similar, with a large basic surface on one side of the barrel (Figure 5(a) and (b)). The basic residues that contribute to the charged surface are located in the phosphorylation loop, in strands 4 and 5, the connecting loop, and the C terminus. The basic surface is on the face of the barrel opposite to the residues shown to be important for binding to PKR are located. The positively charged surface

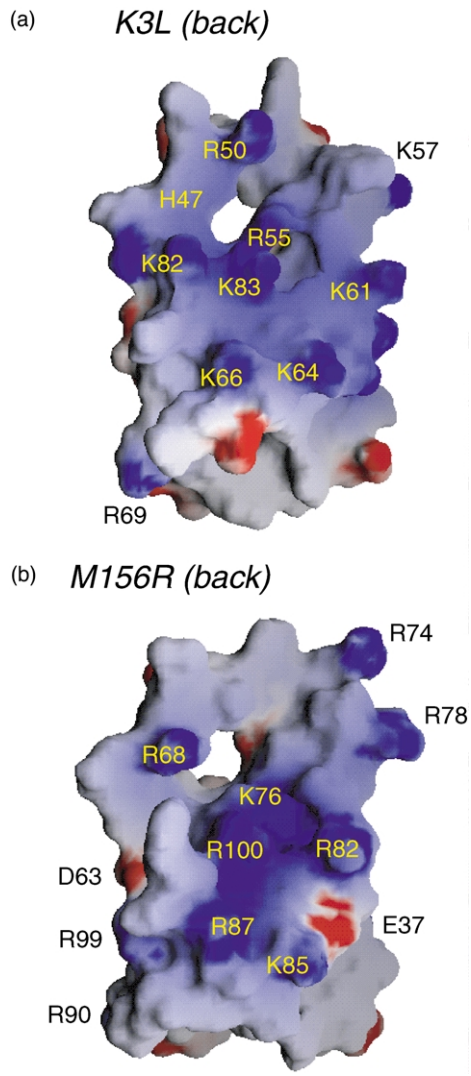

Figure 5. GRASP surface representation of the K3L and M156R structures. (a) Back view of representative K3L homology model (residues 11–83). (b) Back view of selected M156R structure (residues 32–102). Selected basic residues in the C-terminal half of each protein are labeled. The molecular surface is shown in white, and negatively and positively charged side-chains are colored red and blue, respectively.

extends from the helix diagonally down the C-terminal residues and strand 4 towards the conserved Y and D residue in strand 5. Each viral homolog and eIF2α has between eight and 14 basic residues (H, K, or R) in this region that could be important for binding to PKR or another common function.

Discussion

Comparison to structural homologs

A structure similarity search using Dali[22,23] reveals structural similarity to proteins with the OB fold, which consists of five antiparallel β-strands in a closed or partially open barrel with four of the strands following the Greek key motif. These proteins include human eIF2α (*z*-score 4.3), the S1 domain of *Escherichia coli* polynucleotide phosphorylase (PNPase S1 domain) (*z*-score 3.9), the major cold-shock protein (CspA) from *E. coli* (*z*-score 3.8), and the *E. coli* translation initiation factor IF1 (*z*-score 2.1). Most of the structurally similar proteins belong to the nucleic acid-binding domain superfamily in the SCOP database.[24] Proteins with the OB fold often have a low level of sequence similarity but are remarkably similar at the tertiary structure level. Several proteins were predicted to have an S1 motif like that identified in the *E. coli* ribosomal protein S1[25] and characterized for the PNPase S1 domain,[20] including eukaryotic eIF2α and its viral homolog K3L.[20,26]

The M156R structure closely resembles the human eIF2α structure with a backbone r.m.s. deviation of about 2 Å for the superposition of the OB folds, despite the extremely low level of sequence similarity. However, there are some notable differences between the structures. The M156R structure does not contain a β-bulge in strand 1, which is a common feature of OB folds.[20] M156R does contain a conserved Gly before strand 4, another common feature of OB folds. G81 in M156R is the third residue of a four-residue reverse turn and adopts an α_L backbone conformation. In eIF2α, no hydrogen bonding between the parallel β-strands 3 and 5 is present. In M156R, NOE and $^1H/^2H$ exchange data clearly establish the parallel hydrogen bonding pattern. Because of this difference, the barrel of M156R has a slightly smaller diameter, by 1–2 Å, although the lengths of the β-strands are similar. The largest difference in structure is found in the linker between β-strands 3 and 4, which contains the PKR phosphorylation site. In eIF2α, the linker contains one turn of a 3_{10} helix close to strand 3 followed by a large disordered loop, whereas M156R has an α-helix close to strand 4. The difference in the loop structure between these two proteins may reflect the different functional roles of the proteins.

At present, there are 43 proteins with the OB fold in the nucleic acid-binding domain superfamily.[24] Many of these proteins bind to single-stranded DNA (ssDNA) or RNA. Several S1 RNA-binding domains have conserved residues that are clustered on one side of the β-barrel and indicate the likely RNA-binding region.[20] Various prokaryotic cold-shock proteins have conserved residues on the same face, including many solvent-exposed aromatic residues.[27] This evolutionarily conserved binding surface is the expected nucleic acid-binding epitope. The binding face is located on the side of the barrel with the antiparallel strands 2 and 3, the C-terminal end of strand 1, and the loop between strands 4 and 5. On the basis of the Dali alignment between M156R and the PNPase S1 domain or CspA, very few of the aromatic residues are conserved in the viral

homologs of eIF2α or in the N-terminal domain of eIF2α. The missing epitope suggests that the viral homologs and eIF2α are either not involved in nucleic acid binding, or that different residues are involved in binding. This epitope would have been on the same side of the barrel as the regions of M156R that are implicated in binding to PKR with the large basic electrostatic surface on the opposite side. The structural homolog IF1, which has a very low level of sequence similarity to M156R, binds to ribosomal RNA through basic residues in the loop at the top of the barrel.[28] M156R also has basic residues in this loop, including the α-helix, that could mediate nucleic acid binding.

M156R is a substrate and possible inhibitor of PKR

The structure of M156R contains the S1 domain fold that has been determined for the N-terminal domain of eIF2α.[19] It has been hypothesized that the vaccinia virus K3L protein has this fold and that this would allow it to compete for binding to PKR.[5–8] Structural determination of M156R supports this hypothesis for all the viral homologs. Despite the sequence similarity between M156R, C8L, and K3L, it appears that M156R does not function as a PKR inhibitor in the same manner. No phosphorylation of K3L or C8L by PKR has been reported and we have observed no phosphorylation of K3L using the same conditions as the M156R assay (data not shown).

Unlike K3L and C8L, M156R has a Tyr residue (Y67) that aligns with S51 in eIF2α. We showed that M156R can be phosphorylated by PKR *in vitro* and that substitution of Ala for Y67 in M156R substantially reduced phosphorylation. The *in vitro* kinase assay also demonstrated that M156R can compete with eIF2α as a substrate for PKR. Although M156R is a substrate for PKR, it may still be able to inhibit PKR if the phosphorylated form has a slow off-rate from PKR following phosphorylation. As the relative abundance of M156R, eIF2α, and PKR in myxoma virus-infected cells is unknown, it is difficult to predict whether M156R blocks eIF2α phosphorylation in infected cells by a simple competition mechanism. We were unable to detect M156R inhibition of PKR toxicity in yeast; however, it is unclear whether this negative result was due to limitations of the assay, M156R expression or other reasons. Interestingly, mutations designed to make K3L a substrate of PKR eliminated the ability of K3L to inhibit PKR in the yeast assay.[8]

Implications for M156R function

PKR is transcriptionally induced by interferons that are produced by host cells in response to viral invasion. PKR is then activated by dsRNA or specific ssRNA species that bind to the regulatory domain. PKR becomes active by autophosphorylation of several key Ser and Thr residues. Dimerization of the PKR kinase domain is likely required for autophosphorylation, activation, and substrate phosphorylation.[29] The K3L and C8L interaction region has been mapped by *in vitro* and *in vivo* binding studies to the C-terminal region of the PKR catalytic domain.[9–11] *In vitro* studies suggest that K3L can block both kinase autophosphorylation and substrate phosphorylation (T.E.D., unpublished results).[8] Interestingly, the HIV Tat protein is thought to block both PKR autophosphorylation and eIF2α phosphorylation.[30,31] In addition, similar to our findings for M156R, both Tat and the HSV U_s11 protein are reported to be both PKR substrates and inhibitors;[30,32] however, M156R appears to be a significantly better PKR substrate than these other viral proteins.

Some viral inhibitors of PKR act by blocking the kinase catalytic site, while other inhibitors prevent PKR dimerization or interfere with dsRNA binding and activation of PKR.[33] It is possible that M156R plays roles in addition to blocking the active site of PKR. The basic surface of M156R may interact with RNA bound to the PKR regulatory domain, increasing the affinity for activated PKR. Alternatively, M156R could bind to dsRNA through its Arg and Lys rich surface, preventing activation of PKR. The N-terminal 30 residues of M156R have little sequence similarity to the other viral homologs, suggesting a possible unrelated function for these residues for the myxoma virus, such as translational activation of specific mRNAs. In addition, M156R may inhibit other eIF2α kinases in order to maximize viral protein synthesis. Both PKR and HRI were able to phosphorylate eIF2α with a S51Y mutation, demonstrating that their active sites can accommodate the larger Tyr residue.[34]

Regions of eIF2α which are not conserved in the viral homologs may be required for other functions that are not shared. It has been shown recently that phosphorylated eIF2α binds tightly to the regulatory subunits of eIF2B.[35] This interaction involves residues that are important for binding to PKR. Important residues were KG of the KGYID sequence preceding β-strand 5 and residue E50 near the phosphorylation site.[35] These residues are not conserved in M156R, suggesting that M156R does not interact with eIF2B. The phosphorylation loop is another region of eIF2α that is poorly conserved in the viral homologs. This region in eIF2α from mammals, insects, and yeast, is identically conserved over 19 residues, suggesting functional importance. The low sequence similarity suggests that few residues in the loop are necessary for recognition by PKR, although they may be necessary for binding to eIF2B or for an additional function of eIF2α.

Here, we have demonstrated that M156R is a PKR substrate and can compete with eIF2α for phosphorylation by PKR. The structure of M156R provides evidence that in spite of the substantial divergence at the sequence level, M156R is a structural mimic of eIF2α. These studies provide

new insights into the PKR recognition surface on eIF2α and the viral inhibitors, and should be a good resource for further studies on the mechanisms of kinase-substrate recognition and pseudo-substrate inhibition for this important class of translational regulatory protein kinases.

Materials and Methods

Preparation of NMR samples

The M156R gene was PCR amplified from genomic DNA obtained from Dr Grant McFadden (The University of Western Ontario, London, Ontario, Canada) and subcloned into a pET15b vector (Novagen, Madison, WI), which allows the protein to be expressed with an N-terminal His_6 tag followed by a thrombin cleavage site. M156R cloning, protein expression, and the purification method for NMR sample preparation have been described.[36] Proteins were expressed in *E. coli* strain BL21 (Gold λDE3). Cells were grown in 1 l of M9 minimal medium containing $^{15}NH_4Cl$ as the sole nitrogen source, $^{13}C_6$-glucose (3 gm l^{-1}), and supplemented with thiamine and biotin. The cells were grown at 37 °C to an A_{600} of 0.6 and induced with 1 mM IPTG. Afterwards, the temperature was reduced to 15 °C and the cells allowed to grow overnight before harvesting.

Frozen cell pellets were thawed in 500 mM NaCl, 20 mM Tris, 5 mM imidazole (pH 8.0), and lysed by sonication. M156R was extracted from the lysate by batch Ni^{2+} affinity chromatography. The Ni-NTA beads (Qiagen) were washed with 500 mM NaCl, 20 mM Tris, 30 mM imidazole (pH 8.0), and the protein eluted with 500 mM imidazole in this same buffer. M156R was further purified using an SP column (Amersham Pharmacia Biotech). The His_6 tag was cleaved by incubation with thrombin and removed using a Ni-NTA column. Thrombin was removed with a benzamidine Sepharose column (Amersham Pharmacia Biotech). The purified protein was concentrated by ultrafiltration and the buffer exchanged by dilution and reconcentration in the concentrator. The final NMR buffer was 450 mM NaCl, 25 mM Na_2HPO_4, 10 mM DTT, 20 μM Zn^{2+}, 1 mM benzamidine, 1 × inhibitor cocktail (Roche Molecular Biochemicals), and 0.01% (w/v) NaN_3 in 10% (v/v) $^2H_2O/H_2O$ at pH 6.5. The protein concentration was in the range of 0.5–1 mM. The protein was characterized as a monomer by sedimentation equilibrium analysis.

NMR spectroscopy

NMR spectra were recorded at 25 °C on Varian Inova 500, 600, 750 and 800 MHz spectrometers. A 3D HCC-TOCSY-NNH[37–39] spectrum was recorded at 800 MHz. $^1H-^{15}N$ HSQC[40] and 3D ^{15}N-edited NOESY-HQSC[40] (150 ms mixing time) spectra were recorded at 750 MHz. The 2D $^1H-^{13}C$ HSQC,[40] 3D HCCH-TOCSY,[41] CN-NOESY-HSQC[42] (140 ms mixing time), and CBCAC-OCAHA,[43] and 4D CC-NOESY[44] (140 ms mixing time) were recorded at 600 MHz. The HNCA,[45] HN(CO)CA,[45] HNCO,[46] HNCACB,[46] CBCA(CO)NNH,[47] and CCC-TOCSY-NNH[37–39] spectra were recorded at 500 MHz. All the spectra were recorded on a ^{13}C, ^{15}N-labeled sample. The 4D CC-NOESY and $^1H-^{15}N$ HSQC spectra were recorded on this sample after exchange into ^2H_2O. In addition, $^3J_{HNH\alpha}$ values were obtained from a 3D HNHA spectrum recorded on a ^{15}N-labeled sample at 600 MHz as described.[48] Total data acquisition time was 48 days. Spectra were processed and analyzed with Felix97 (Molecular Simulations Inc.) and Sparky†.

Structure calculations

Solution structures were calculated with the restraint parameters given in Table 1. Hydrogen-bond distance restraints were used on the basis of identification of slow-exchanging peaks in a $^1H-^{15}N$ HSQC spectrum recorded in ^2H_2O approximately five hours after exchange (two restraints per hydrogen-bond). NOEs were classified as strong (1.8–2.5 Å), medium (1.8–3.5 Å), or weak (1.8-5 Å) according to estimated peak volumes for sequential NOEs. Medium or long-range NOEs involving side-chain protons were given the longest upper bound (5 Å) unless they were very strong (4 Å). Pseudoatom corrections were added to upper bound restraint for methyl, methylene groups (1 Å), unresolved H^δ or H^ε protons of Phe or Tyr (2.4 Å), and non-sterospecifically assigned Leu and Val methyl groups (2.4 Å). Dihedral angle restraints were used when preliminary structure calculations clearly indicated α-helix or β-strand secondary structure and $^3J_{HNH\alpha}$ measurements did not disagree. Solution structures were calculated using a standard distance geometry/simulated annealing protocol[49] implemented by the program X-PLOR 3.84.[50]

Protein kinase assays

His_6-tagged M156R and M156R-Y67A proteins were expressed in *E. coli* strain BL21-Gold(DE3) pLysS (Stratagene). Cells were grown in 500 ml of LB medium at 37 °C to A_{600} of 0.8 and induced with 0.25 mM IPTG for 3.5 hours at 30 °C. Cells were harvested and broken with sonication in 50 mM Na_2HPO_4, 300 mM NaCl, 15 mM imidazole, 10 mM 2-mercaptoethanol, 1 mM PMSF and 1 × protease inhibitor cocktail (Roche Molecular Biochemicals) at pH 8.0. The supernatants of the cell lysates were incubated with Ni-NTA agarose beads (Qiagen) for one hour at 4 °C. Beads were washed three times with 50 mM Na_2HPO_4, 300 mM NaCl, 20 mM imidazole, and 10 mM 2-mercaptoethanol (pH 8.0). Proteins were eluted from the beads with 50 mM Na_2HPO_4, 300 mM NaCl, 250 mM imidazole, 10 mM 2-mercaptoethanol (pH 8.0), and dialyzed against 50 mM Tris–HCl (pH 8.0), 250 mM NaCl, 10 mM KCl, 2 mM DTT and 20% (v/v) glycerol.

Flag and His_6-tagged PKR was purified as described;[35] and the purified protein was dialyzed against 20 mM Tris–HCl (pH 8.0), 100 mM NaCl, 10 mM $MgCl_2$, 0.1 mM EDTA, 1 mM DTT and10% glycerol. His-tagged yeast eIF2α (residues 1–200) and eIF2α-S51A were purified as described,[51] and stored in the same buffer as the M156R proteins.

In vitro phosphorylation reactions were carried out in 50 μl of 20 mM Tris–HCl (pH 8.0), 50 mM KCl, 25 mM $MgCl_2$, 1 mM DTT, 10 μM ATP containing 5 μCi of [γ-^{33}P]ATP, 1 μM PMSF and 1 × protease inhibitor cocktail for 30 minutes at room temperature. Reactions were terminated by adding SDS sample buffer and boiling for five minutes, and samples were analyzed by Tris–glycine SDS/4–20% polyacrylamide gel electrophoresis.

† http://www.cgl.ucsf.edu/home/sparky

Gels were dried and phosphorylated proteins were detected by autoradiography.

LC-MS/MS analysis

The proteins were separated eletrophoretically using SDS-PAGE and the Coomassie-stained bands corresponding to phosphorylated and native M156R (~5 μg each) were excised then destained using 1:1 (v/v) CH_3CN/50 mM NH_4HCO_3 at pH 8.3. The destained gel slices were dried using a SpeedVac concentrator (Thermo Savant, San Jose, CA), rehydrated with 50 mM NH_4HCO_3 (pH 8.3), crushed into smaller pieces, and then dried. The gel pieces were rehydrated with a 30 μl of 50 mM NH_4HCO_3 (pH 8.3), containing enough trypsin to provide a 1:5 (w/w) trypsin-to-protein ratio and then incubated overnight at 37 °C. After proteolysis, the peptides were extracted three times by adding 0.2 ml of 60% CH_3CN, 0.1% (v/v) trifluoroacetic acid to each sample and then sonicating for 30 minutes in a sonicating bath. The pooled extracts were dried and stored at −80 °C.

LC-MS/MS analysis of the in-gel digested samples was performed using an Agilent 1100 Series capillary LC system (Agilent Technologies, Inc., Palo Alto, CA) coupled directly on-line with a Deca-LCQ ion-trap mass spectrometer (Thermo Finnigan, San Jose, CA) using an in-house manufactured electrospray interface. The reversed-phase capillary HPLC column contained 5 μm Jupiter C_{18} stationary phase (Phenomenex, Torrence, CA) packed into a 360 μm o.d. × 150 μm i.d. × 60 cm length capillary (Polymicro Technologies Inc., Phoenix, AZ). The mobile phase consisted of (A) 0.1% (v/v) formic acid in water and (B) 0.1% (v/v) formic acid in CH_3CN. After injecting a sample volume of 8 μl onto the reversed-phase column, the mobile phase was held at 5% B for 20 minutes followed by a linear gradient to 70% B over 80 minutes and a linear gradient to 85% B over 45 minutes at a flow-rate of 1.5 μl min^{-1}.

The data acquisition sequence used for all LC-MS/MS analyses employed a full MS scan followed by three MS/MS scans, where the three most intense ions were selected dynamically from the precursor MS scan and subjected to collision-induced dissociation using a normalized collision energy setting of 45%. Peptides were identified by searching the MS/MS spectra against a database containing the M156R sequence using SEQUEST (Thermo Finnigan, San Jose, CA). All of the spectra were analyzed using a dynamic mass modification on Ser, Thr, and Tyr residues equal to the additional monoisotopic mass of HPO_3 (79.966 Da). In addition, all oxidation states of Met and Cys were used as static modifications to identify oxidized peptides.

Illustrations

Figures were drawn using the programs InsightII (Molecular Simulations Inc.), MOLSCRIPT,[52] Raster3D,[53] and GRASP.[54]

Data Bank accession numbers

An ensemble of 20 structures has been deposited in the Protein Data Bank under accession number 1JJG. The backbone and side-chain chemical shift assignments (^1H, ^{13}C, and ^{15}N) have been deposited at the BioMagResBank under accession code 5077.

Acknowledgements

We thank Madhusudan Dey for help with PKR and eIF2α purification. Acquisition and processing of NMR spectra and structure calculations were performed in the Environmental Molecular Sciences Laboratory (a national scientific user facility sponsored by the US DOE Office of Biological and Environmental Research) located at Pacific Northwest National Laboratory and operated for DOE by Battelle. This work was supported by DOE (grant KP1104010) and NIH Protein Structure Initiative Northeast Structural Genomics Consortium (NIH grant P50-GM62413). T.A.R. acknowledges support from a postdoctoral fellowship from Associated Western Universities, Northwest Division.

References

1. Cameron, C., Hota-Mitchell, S., Chen, L., Barrett, J., W, ., Cao, J.-X., Macaulay, C. *et al.* (1999). The complete DNA sequence of myxoma virus. *Virology*, **264**, 298–318.
2. Barrett, J. W., Cao, J.-X., Hota-Mitchell, S. & McFadden, G. (2001). Immunomodulatory proteins of myxoma virus. *Semin. Immunol.* **13**, 73–84.
3. Ploegh, H. L. (1998). Viral strategies of immune invasion. *Science*, **280**, 248–253.
4. Spriggs, M. K. (1996). One step ahead of the game: viral immunomodulatory molecules. *Annu. Rev. Immunol.* **14**, 101–131.
5. Beattie, E., Tartaglia, J. & Paolettit, E. (1991). Vaccinia virus-encoded eIF-2α homolog abrogates the antiviral effect of interferon. *Virology*, **183**, 419–422.
6. Carroll, K., Elroy-Stein, O., Moss, B. & Jagus, R. (1993). Recombinant vaccinia virus K3L gene product prevents activation of double-stranded RNA-dependent, initiation factor 2α-specific protein kinase. *J. Biol. Chem.* **268**, 12837–12842.
7. Davies, M. V., Elroy-Stein, O., Jagus, R., Moss, B. & Kaufman, R. J. (1992). The vaccinia virus K3L gene product potentiates translation by inhibiting double-stranded-RNA-activated protein kinase and phosphorylation of the α subunit of eukaryotic initiation factor II. *J. Virol.* **66**, 1943–1950.
8. Kawagishi-Kobayashi, M., Silverman, J. B., Ung, T. L. & Dever, T. E. (1997). Regulation of the protein kinase PKR by the vaccinia virus pseudosubstrate inhibitor K3L is dependent on residues conserved between the K3L protein and the PKR substrate eIF2α. *Mol. Cell Biol.* **17**, 4146–4158.
9. Kawagishi-Kobayashi, M., Cao, C., Lu, J., Ozato, K. & Dever, T. E. (2000). Pseudosubstrate inhibition of protein kinase PKR by swine pox virus C8L gene product. *Virology*, **276**, 424–434.
10. Gale, M. J., Seng-Lai, T., Wambach, M. & Katze, M. G. (1996). Interaction of the interferon-induced PKR protein kinase with inhibitory proteins $P58^{IPK}$ and vaccinia virus K3L is mediated by unique domains: implications for kinase regulation. *Mol. Cell Biol.* **16**, 4172–4181.
11. Sharp, T. V., Witzel, J. E. & Jagus, R. (1997). Homologous regions of the α subunit of eukaryotic translational initiation factor 2 (eIF2α) and the vaccinia virus K3L gene product interact with the

same domain within the dsRNA-activated protein kinase (PKR). *Eur. J. Biochem.* **250**, 85–91.
12. Hinnebusch, A. G. (2000). Mechanism and regulation of initiator methionyl-tRNA binding to ribosomes. In *Translational Control of Gene Expression* (Sonenberg, N., Hershey, J. W. B. & Mathews, M. B., eds), pp. 185–243, Cold Spring Harbor Laboratory Press, Cold Spring Harbor, NY.
13. Gale, M. J. & Katze, M. G. (1998). Molecular mechanisms of interferon resistance mediated by viral-directed inhibition of PKR, the interferon-induced protein kinase. *Pharmacol. Ther.* **78**, 29–46.
14. Dever, T. E. (2002). Gene-specific regulation by general translation factors. *Cell*, **108**, 545–556.
15. Ron, D. & Harding, H. P. (2000). PERK and translational control by stress in the endoplasmic reticulum. In *Translational Control of Gene Expression* (Sonenberg, N., Hershey, J. W. B. & Mathews, M. B., eds), pp. 547–560, Cold Spring Harbor Laboratory Press, Cold Spring Harbor, NY.
16. Chen, J. J. & London, I. (1995). Regulation of protein synthesis by heme-regulated eIF-2α kinase. *Trends Biochem. Sci.* **20**, 105–108.
17. Qian, W., Zhu, S., Sobolev, A. & Wek, R. C. (1996). Expression of vaccinia virus K3L protein in yeast inhibits eukaryotic initiation factor-2 kinase GCN2 and the general amino acid control pathway. *J. Biol. Chem.* **271**, 13202–13207.
18. Sood, R., Porter, A. C., Ma, K., Quilliam, L. A. & Wek, R. C. (2000). Pancreatic eukaryotic initiation factor-2α kinase (PEK) homologues in humans, *Drosophila melanogaster* and *Caenorhabditis elegans* that mediate translational control in response to endoplasmic reticulum stress. *Biochem. J.* **346**, 281–293.
19. Nonato, M. C., Widom, J. & Clardy, J. (2002). Crystal structure of the N-terminal segment of human eukaryotic translation initiation factor 2α. *J. Biol. Chem.* **277**, 17057–17061.
20. Bycroft, M., Hubbard, T. J. P., Proctor, M., Freund, S. M. V. & Murzin, A. G. (1997). The solution structure of the S1 RNA-binding domain: a member of an ancient nucleic acid-binding fold. *Cell*, **88**, 235–242.
21. Li, H., Tejero, R., Monleon, D., Bassolino-Klimas, D., Abate-Shen, C., Bruccoleri, R. E. & Montelione, G. T. (1997). Homology modeling using simulated annealing of restrained molecular dynamics and conformational search calculation with CONGEN: application in predicting the three-dimensional structure of murine homeodomain Msx-1. *Protein Sci.* **6**, 956–970.
22. Holm, L. & Sander, C. (1993). Protein structure comparison by alignment of distance matrices. *J. Mol. Biol.* **233**, 123–138.
23. Holm, L. & Sander, C. (1996). Mapping the protein universe. *Science*, **273**, 595–602.
24. Murzin, A. G., Lo Conte, L., Ailey, B. G., Brenner, S. E., Hubbard, T. J. P. & Cothia, C. (1995). SCOP: a structural classification of proteins database for the investigation of sequences and structures. *J. Mol. Biol.* **247**, 536–540.
25. Subramanian, A. R. (1983). Structure and functions of ribosomal protein S1. *Prog. Nucl Acid Res. Mol. Biol.* **28**, 101–142.
26. Gribskov, M. (1992). Translational initiation factors IF1 and eIF2α share an RNA-binding motif with prokaryotic ribosomal protein S1 and polynucleotide phosphorylase. *Gene*, **119**, 107–111.
27. Feng, W., Tejero, R., Zimmerman, D. E., Inouye, M. & Montelione, G. T. (1998). Solution NMR structure and backbone dynamics of the major cold-shock protein (CspA) from *Escherichia coli*: evidence for conformational dynamics in the single-stranded RNA-binding site. *Biochemistry*, **37**, 10881–10896.
28. Carter, A. P., Clemons, W. M., Jr, Brodersen, D. E. B., Morgan-Warren, R. J., Hartsch, T., Wimberly, B. T. & Ramakrishnan, V. (2001). Crystal structure of an initiation factor bound to the 30S ribosomal subunit. *Science*, **291**, 498–501.
29. Ung, T. L., Cao, C., Lu, J., Ozato, K. & Dever, T. E. (2001). Heterologous dimerization domains functionally substitute for the double-stranded RNA-binding domains of the kinase PKR. *EMBO J.* **20**, 3728–3737.
30. Brand, S. R., Kobayashi, R. & Mathews, M. B. (1997). The TAT protein of human immunodeficiency virus type 1 is a substrate and inhibitor of the interferon-induced, virally activated protein kinase, PKR. *J. Biol. Chem.* **272**, 8388–8395.
31. Cai, R., Carpick, B., Chun, R. G., Jeang, K.-T. & Williams, B. R. G. (2000). HIV-1 TAT inhibits PKR activity by both RNA-dependent and RNA-independent mechanisms. *Arch. Biochem. Biophys.* **373**, 361–367.
32. Cassady, K. A., Gross, M. & Roizman, B. (1998). The herpes simplex virus U_S11 protein effectively compensates for the $g_1$34.5 gene if present before activation of protein kinase R by precluding its phosphorylation and that of the α subunit of eukaryotic translation initiation factor 2. *J. Virol.* **72**, 8620–8626.
33. Gale, M. J., Seng-Lai, T. & Katze, M. G. (2000). Translational control of viral gene expression in eukaryotes. *Microbiol. Mol. Biol. Rev.* **64**, 239–280.
34. Lu, J., O'Hara, E. B., Trieselmann, B. A., Romana, P. R. & Dever, T. E. (1999). The interferon-induced double-stranded RNA-activated protein kinase PKR will phosphorylate serine, threonine, or tyrosine at residue 51 in eukaryotic initiation factor 2α. *J. Biol. Chem.* **274**, 32198–32203.
35. Krishnamoorthy, T., Pavitt, G. D., Zhang, F., Dever, T. E. & Hinnebusch, A. G. (2001). Tight binding of the phosphorylated α subunit of initiation factor 2 (eIF2α) to the regulatory subunits of guanine nucleotide exchange factor eIF2B is required for inhibition of translation initiation. *Mol. Cell Biol.* **21**, 5018–5030.
36. Yee, A., Chang, X., Pineda-Lucena, A., Wu, B., Semesi, A., Le, B. *et al.* (2002). An NMR approach to structural proteomics. *Proc. Natl Acad. Sci. USA*, **99**, 1825–1830.
37. Logan, T. M., Olejniczak, E. T., Xu, R. X. & Fesik, S. W. (1993). A general method for assigning NMR spectra of denatured proteins using 3D HC(CO)NH-TOCSY triple resonance experiments. *J. Biomol. NMR*, **3**, 225–231.
38. Grzesiek, S., Anglister, J. & Bax, A. (1993). Correlation of backbone and amide and aliphatic side-chain resonances in $^{13}C/^{15}N$-enriched proteins by isotropic mixing of ^{13}C magnetization. *J. Magn. Reson. ser. B*, **101**, 114–119.
39. Montelione, G. T., Lyons, B. A., Emerson, S. D. & Tashiro, M. (1992). An efficient triple resonance experiment using carbon-13 isotropic mixing for determining sequence-specific resonance assignments of isotopically enriched proteins. *J. Am. Chem. Soc.* **114**, 10974–10975.
40. Zhang, O., Kay, L. E., Olivier, J. P. & Forman-Kay, J. D. (1994). Backbone ^{1}H and ^{15}N resonance assignments of the N-terminal SH3 domain of Drk in folded and

unfolded states using enhanced-sensitivity pulsed field gradient NMR techniques. *J. Biomol. NMR*, **4**, 845–858.
41. Kay, L. E., Xu, G. Y., Singer, A. U., Muhandiram, D. R. & Forman-Kay, J. D. (1993). A gradient-enhanced HCCH TOCSY experiment for recording side-chain ^{1}H and ^{13}C correlations in H_2O samples of proteins. *J. Magn. Reson. ser. B*, **101**, 333–337.
42. Pascal, S. M., Muhandiram, D. R., Yamazaki, T., Forman-Kay, J. D. & Kay, L. E. (1994). Simultaneous acquisition of ^{15}N-edited and ^{13}C-edited NOE spectra of proteins dissolved in H_2O. *J. Magn. Reson. ser. B*, **103**, 197–201.
43. Kay, L. E. (1993). Pulsed-field gradient-enhanced three-dimensional NMR experiment for correlating $^{13}C\alpha/\beta$, $^{13}C'$, and $^{1}H\alpha$ chemical shifts in uniformly ^{13}C-labeled proteins dissolved in H_2O. *J. Am. Chem. Soc.* **115**, 2055–2057.
44. Vuister, G. W., Clore, G. M., Gronenborn, A. M., Powers, R., Garrett, D. S., Tschudin, R. & Bax, A. (1993). Increased resolution and improved spectral quality in 4-dimensional $^{13}C/^{13}C$-separated HMQC-NOESY-HMQC spectra using pulsed-field gradients. *J. Magn. Reson. ser. B*, **101**, 210–213.
45. Yamazaki, T., Lee, W., Arrowsmith, C. H., Munhandiram, D. R. & Kay, L. E. (1994). A suite of triple-resonance NMR experiments for the backbone assignment of ^{15}N, ^{13}C, ^{2}H labeled proteins with high-sensitivity. *J. Am. Chem. Soc.* **116**, 11655–11666.
46. Muhandiram, D. R. & Kay, L. E. (1994). Gradient-enhanced triple-resonance three-dimensional NMR experiments with improved sensitivity. *J. Magn. Reson. ser. B*, **103**, 203–216.
47. Grzesiek, S. & Bax, A. (1992). Correlating backbone amide and side-chain resonances in larger proteins by multiple relayed triple resonance NMR. *J. Am. Chem. Soc.* **114**, 6291–6293.
48. Vuister, G. W. & Bax, A. (1993). Quantitative *J* correlation: a new approach for measuring homonuclear three-bond JHNHα coupling constants in ^{15}N-enriched proteins. *J. Am. Chem. Soc.* **115**, 7772–7777.
49. Nilges, M., Clore, G. M. & Gronenborn, A. M. (1988). Determination of 3-dimensional structures of proteins from interproton distance data by hybrid distance geometry-dynamical simulated annealing calculations. *FEBS Letters*, **229**, 317–324.
50. Brünger, A. T. (1992). *X-PLOR Version 3.1: A System for X-ray Crystallography and NMR*, Yale University Press, New Haven, CT.
51. Zhu, S., Sobolev, A. Y. & Wek, R. C. (1996). Histidyl-tRNA synthetase-related sequences in GCN2 protein kinase regulate *in vitro* phosphorylation of eIF-2. *J. Biol. Chem.* **271**, 24989–24994.
52. Kraulis, P. J. (1991). MOLSCRIPT: a program to produce both detailed and schematic plots of protein structures. *J. Appl. Crystallog.* **24**, 946–950.
53. Merritt, E. A. & Bacon, D. J. (1997). Raster3D: photorealistic molecular graphics. *Methods Enzymol.* **277**, 505–524.
54. Nicholls, A., Sharp, K. A. & Honig, B. (1991). GRASP—graphical representation and analysis of surface-properties. *Proteins: Struct. Funct. Genet.* **11**, 281–296.
55. Willer, D. O., McFadden, G. & Evans, D. H. (1999). The complete genome sequence of shope (rabbit) fibroma virus. *Virology*, **264**, 319–343.
56. Massung, R. F., Jayarama, V. & Moyer, R. W. (1993). DNA sequence analysis of conserved and unique regions of swinepox virus: identification of genetic elements supporting phenotypic observations including a novel G protein-coupled receptor homologue. *Virology*, **197**, 511–528.
57. Boursnell, M. E., Foulds, I. J., Campbell, J. I. & Binns, M. M. (1988). Non-essential genes in the vaccinia virus HindIII K fragment: a gene related to serine protease inhibitors and a gene related to the 37 K vaccinia virus major envelope antigen. *J. Gen. Virol.* **69**, 2995–3003.
58. Shchelkunov, S. N., Blinov, V. M. & Sandakhchiev, L. S. (1993). Genes of variola and vaccinia viruses necessary to overcome the host protective mechanisms. *FEBS Letters*, **319**, 80–83.
59. Ernst, H., Duncan, R. F. & Hershey, J. W. (1987). Cloning and sequencing of complementary DNAs encoding the α-subunit of translational initiation factor eIF-2. Characterization of the protein and its messenger RNA. *J. Biol. Chem.* **262**, 1206–1212.
60. Laskowski, R. A., Rullmann, J. A., MacArthur, M. W., Kaptein, R. & Thornton, J. M. (1996). AQUA and PROCHECK-NMR: programs for checking the quality of protein structures solved by NMR. *J. Biomol. NMR*, **8**, 447–486.

Edited by M. F. Summers

(Received 20 May 2002; received in revised form 12 August 2002; accepted 12 August 2002)

Note added in proof: While this manuscript was in press, the vaccinia virus K3L crystal structure was deposited in the PDB (accession number 1LUZ). (Dar, A. C. & Sicheri, F. (2002). *Mol. Cell*, **10**, 295–305.)